Systematic study of incomplete-fusion dynamics below 8 MeV/nucleon energy

Harish Kumar,[1,*] Suhail A. Tali,[1] M. Afzal Ansari,[1,†] D. Singh,[2] Rahbar Ali,[3] Asif Ali,[1] Siddharth Parashari,[1] Pankaj K. Giri,[2] Sneha B. Linda,[2] R. Kumar,[4] R. P. Singh,[4] and S. Muralithar[4]

[1]*Nuclear Physics Laboratory, Department of Physics, Aligarh Muslim University, Aligarh 202002, India*

[2]*Centre for Applied Physics, Central University of Jharkhand, Ranchi 835205, India*

[3]*Department of Physics, Gandhi Faiz-E-Aam College, Shahajhanpur 242001, India*

[4]*Nuclear Physics Group, Inter University Accelerator Centre, New Delhi 110067, India*

(Received 23 June 2018; revised manuscript received 17 January 2019; published 18 March 2019)

An attempt has been made to provide crucial information about the dependence of incomplete-fusion dynamics on various entrance channel parameters below 8 MeV/nucleon energy. The forward recoil range distributions of several evaporation residues produced in the $^{13}C + ^{175}Lu$ system have been measured at ≈88-MeV energy and examined in the framework of the code SRIM. Owing to the fractional linear momentum transfer from the projectile to the target nucleus, incomplete-fusion (ICF) products are observed to be trapped at lower cumulative thickness than that of complete fusion products. In order to study the incomplete-fusion behavior with various entrance channel parameters, the incomplete-fusion fraction (F_{ICF}) has also been deduced and compared with those obtained for the systems available in the literature. The reinvestigation of the Coulomb factor ($Z_P Z_T$) dependence of incomplete fusion indicates that it is somehow projectile structure dependent. No systematic trend is observed with the target deformation parameter (β_2) dependent study of ICF. A systematic linear growth in the incomplete-fusion probability function (F_{ICF}) is observed with increasing the parameters $Z_P Z_T \beta_2$ and $Z_P Z_T/(1-\beta_2)$, but separately for α- and non-α-cluster structured projectiles with different targets. The present findings explore the role of Coulomb interaction on ICF dynamics more effectively. Moreover, the projectile α-Q value is found to be a suitable parameter which explains effectively the observed trend in the study of ICF with the above-mentioned parameters. The incomplete-fusion existence below critical angular momentum (ℓ_{crit}), i.e., $\ell \leqslant \ell_{crit}$, is also observed for the present $^{13}C + ^{175}Lu$ system.

DOI: 10.1103/PhysRevC.99.034610

I. INTRODUCTION

Efforts are continuously being made to investigate the incomplete-fusion (ICF) process in collisions of heavy ions at lower projectile energies [1–5]. In the interaction of two heavy ions, several reaction channels may open up, which further leads to the transfer of cluster of the nucleons. Fusion suppression based studies have also explored the ICF dynamics, using weakly bound projectiles around the barrier [6–9]. Nevertheless, the study of ICF is still an active area of research due to complexity in the mass transferred from the projectile to the target. Thereby, it requires further investigation to unfold the ICF dependence on various entrance channel parameters. It is now a well-understood fact that the ICF process is also one of the dominant reaction modes other than complete fusion (CF) at energies near and well above the Coulomb barrier (V_{CB}), which contributes significantly to the total fusion cross sections [10–13]. In the case of CF, the entire projectile fuses with the target nucleus. On the other hand, the incident projectile may break up into its fragments in the case of ICF, wherein only one of the parts fuses with the target and the remnant moves as a spectator.

The experimental features of the ICF in the breakup of projectiles like ^{12}C, ^{14}N, and ^{16}O into α clusters were first observed by Britt and Quinton [14]. However, Inamura *et al.* [15] provided the major advances in the study of the ICF process from the extracted information based on the particle-γ coincidence measurements. Udagawa and Tamura [16] explained the projectile breakup into α clusters in the vicinity of the target nuclear field. Several theoretical models [16–20] were proposed using tightly bound projectiles to explain the ICF process. The CF and the ICF processes have also been categorized on the basis of imparted angular momentum (ℓ) in the system. For the ICF process, the attractive nuclear potential is no longer strong enough to capture the projectile entirely by the target nucleus and the CF gives way to the ICF process. As per predictions of the SUMRULE model of Wilczynski *et al.* [17], the ICF process exists only for input angular momentum values (ℓ) greater than critical angular momentum values (ℓ_{crit}). However, in contradiction to the SUMRULE model approach, a substantial contribution of ICF below ℓ_{crit} has also been observed in recent studies [12,13,21–23]. As the projectile partially fuses with the target, less nucleonic degrees of freedom participate in the case of ICF. Hence, owing to the linear momentum transfer (LMT), the ICF products are observed to traverse the shorter path in the stopping medium compared with that of CF products [4,12,22,23]. The studies available in the literature show noticeable ICF contribution in the

*amu.harish@gmail.com

†drmafzalansari@yahoo.com

α-emission channel products [4,5,10–13,21–23]. The forward recoil range distribution (FRRD) measurement is observed to be a sensitive probe to differentiate the residues produced by the CF and/or the ICF processes on the basis of their recoil ranges [4,12,22,23]. The proposed theoretical models [16–20] using tightly bound projectiles explain satisfactorily the ICF process above 10 MeV/nucleon energy. Theoretical works have also addressed the low-energy breakup fusion reactions of weakly bound projectiles by using the quantum and classical approaches [24–28]. The effect of continuum couplings in the fusion is studied using a three-body model within continuum-discretized coupled-channel (CDCC) formalism around the Coulomb barrier energies [24,25]. The existing quantum models have limitations, as they cannot calculate integrated CF and ICF cross sections unambiguously. Neither, after the formation of ICF products, can these follow the evolution of the surviving breakup fragment(s) since ICF results in depletion of the total few-body wave function. Nevertheless, some difficulties are overcome by the classical dynamical reaction model suggested in Ref. [26]. The comparison of breakup observables with CDCC quantum-mechanical predictions is taken into account in this model. Further improvements have also been made in this classical model in later studies [27–29]. In these studies, the key new aspect is the time propagation of the surviving breakup fragment and the ICF product. A self-contained PLATYPUS code [28] based on a three-dimensional classical dynamical reaction model with stochastic breakup has been implemented, which is a useful tool for quantifying CF and ICF and breakup in weakly bound two-body projectile induced reactions near the Coulomb barrier. This code calculates the integrated CF and ICF cross sections and their angular momentum distribution, the excitation energy distribution of the primary ICF products, the asymptotic angular distribution of ICF products, and the surviving breakup fragments as well as breakup observables such as angle, kinetic energy, and relative energy distributions. A few required additions to the original version of the PLATYPUS code are explained in Ref. [29], followed by a discussion about model calculations for ICF in collisions of ^{6}Li with ^{209}Bi above the Coulomb barrier energies. The classical model [26–29] does not include the quantum tunneling probability. To overcome this problem, a quantum reaction approach to low-energy breakup reactions of weakly bound nuclei based on the time-dependent wave-packet method was presented in Ref. [30]. The improved version of a semiclassical coupled-channel method previously developed to evaluate fusion cross sections in collisions of weakly bound nuclei is provided in Ref. [31]. This version takes into account the static effects of the low breakup threshold, uses better bin states in the discretization of the continuum, and avoids the excitation of closed channels.

Several ICF studies have been made in recent years, but the ambiguous dependence of ICF on different parameters needs serious attention. Hinde *et al.* [32] suggested that the fusion suppression is almost proportional to the target charge Z_T. However, Rafiei *et al.* [33] observed the nondependency of the ICF probability with the target charge (Z_T). Morgenstern *et al.* [34] correlated the CF probability with the projectile-target mass asymmetry [$A_T/(A_P + A_T)$]. Recently, it was observed that Morgenstern *et al.*'s mass-asymmetry systematic is somehow a projectile structure dependent [21,23]. Apart from this, the effect of projectile structure on the ICF process has also been observed by Singh *et al.* [35] and Babu *et al.* [36]. The observed projectile structure effect on ICF is explored more effectively in terms of projectile α-Q value [12,21,23,37,38]. Shuaib *et al.* [39] reported that ICF probability increases linearly with increasing the product of projectile and target charges Z_PZ_T (Coulomb factor). On the other hand, the reinvestigation of Coulomb factor dependence of ICF reveals that ICF behavior with the Coulomb factor follows linear trends but separately for each projectile [40,41]. Gerschel [42] and Singh *et al.* [11] studied the role of target deformation in incomplete-fusion dynamics on the basis of the localization of the ℓ window. Some discrepancy is observed in the incomplete-fusion dependence on the target deformation parameter (β_2), which is further correlated with a new parameter $Z_PZ_T\beta_2$ in our recent work [41]. The ICF study based on this parameter dependence is limited only for a very few systems. It is also noteworthy that despite the majority of fusion suppression based works using loosely bound projectiles carried out earlier [6–8,43] some work has also been done using tightly bound projectiles [44,45]. In the recently reported studies based on FRRD measurement [44,45], it is also observed that the extent of fusion suppression may be governed by projectile breakup threshold energy ($E_{\rm BU}$). Muntazir *et al.* [45] also explored the role of Coulomb repulsion in the breakup fusion reactions by comparing the fusion suppression data of different ^{16}O induced reactions in the light of the empirical formula suggested by Hinde *et al.* [32]. Moreover, the ICF dependency on various entrance channel parameters has been considered to be the field of keen interest to reach some definite conclusion.

In the present paper, with a motivation of better insight into the ICF dependence on various entrance channel parameters, the FRRDs of residues produced in the ^{13}C + ^{175}Lu systems have been measured at ≈88-MeV energy. The measured FRRDs are analyzed in the framework of the Stopping Power and Range of Ions in Matter (SRIM) code [46]. The FRRD measurement gives a better understanding of different degrees of LMT associated with CF and/or ICF. From the present data analysis, the relative contribution due to different fusion components has been separated out. The ICF probability function ($F_{\rm ICF}$) deduced from the present paper has been compared with those obtained for the systems available in the literature. The present analysis includes the systematic study of ICF dependence on the Coulomb factor (Z_PZ_T), target deformation parameter (β_2), parameters $Z_PZ_T\beta_2$, $Z_PZ_T/(1-\beta_2)$, and the projectile α-Q value. The present results support the recently observed Coulomb factor Z_PZ_T based findings [40,41] and are also in good agreement with our recent observations [41] based on parameter $Z_PZ_T\beta_2$. The parameter $Z_PZ_T/(1-\beta_2)$ is found more suitable for the understanding of ICF dependence on target deformation. This paper also indicates that the projectile α-Q value also seems to be an important parameter in the study of α- and non-α-cluster structured projectile induced reactions. It is also observed that the fusion ℓ distribution window suggested in the SUMRULE model [17] is a broad diffused boundary. It is also noteworthy that the FRRDs of

evaporation residues (ERs) are measured and reported for the first time, to the best of our knowledge, by using the projectile ^{13}C. In the light of recently reported observations based on FRRD measurement [44,45], the present paper in turn may be helpful in bridging the gap between the ICF studies of tightly and weakly bound projectiles at energies above the Coulomb barrier. This paper is organized in the following sections. Section II includes the experimental details, Sec. III presents the analysis of measured FRRDs, and the ICF correlation with various parameters is given in Sec. IV. Section V presents the conclusions obtained from the present paper.

II. EXPERIMENTAL PROCEDURE

The experiment was performed by using the stacked foil activation technique [47] at Inter University Accelerator Centre (IUAC), New Delhi, India. The self-supporting natural ^{175}Lu target (purity $\approx$ 97.41%) of thickness $\approx$960 μg/cm^2 was followed by a series of thin Al-catcher foils having thickness range $\approx$24−45 μg/cm^2. Rolling technique was used for the preparation of target foil. However, the thin Al-catcher foils which serve as stopping medium were fabricated by vacuum evaporation technique. The target thickness was determined by using the α-transmission procedure and also the weighing method. The uniformity of the target was also verified by α-transmission method. However, only the α-transmission procedure was adopted for the measurement of the thin Al-catcher foil thickness. The irradiation of the ^{175}Lu target with the ^{13}C ion beam for about 16 h at $\approx$88-MeV energy was carried out in the General Purpose Scattering Chamber, which has an in-vacuum transfer facility (ITF). It is worth mentioning that the ITF is used to minimize the time lapse between the end of irradiation and the start of the counting of the irradiated sample. The incident projectile energy at half target thickness was calculated by using the code SRIM [46]. The Al-catcher foil thickness was chosen in such a way that a complete range profile may be achieved and all the recoiling residues get trapped at their respective catcher foil thicknesses. Beam flux was estimated by using the total charge collected in the Faraday cup, which was kept behind the target-catcher assembly.

A precalibrated HPGe detector of 100-cc active volume coupled to the PC through CAMAC based FREEDOM software [48] was used for recording the induced γ-ray activities in each Al-catcher foil. The counting was made separately at increasing intervals of time, keeping in view the half-lives of the populated residues and their identification in the decay curve analysis. The standard ^{152}Eu γ-ray source of known strength was used for the energy calibration and also to determine the efficiency of the HPGe detector. The energy resolution of the detector was found to be $\approx$2.5 keV for the 1408-keV γ ray of the standard source. During the measurement, the dead time of the detector was kept $\leqslant$ 10%. The geometry dependent efficiency of the detector was calculated by using the standard γ-ray source at same source-to-detector distance as that for the Al-catcher foils to wash out the solid angle effect. Further, the populated residues were identified on the basis of their characteristic γ-ray energies in the decay curve analysis. It is noteworthy that the production cross sections $\sigma_r(E)$ provide the comprehensive information about the formation of any particular evaporation residue. In the present paper, the cross sections have been determined from the measured intensities of each γ ray by using the standard formulation [49]. The factors like the target nonuniformity, the beam current fluctuations, finite dead time, and the uncertainty in the geometry dependent detection efficiencies of the detector may evoke the errors in the measured cross sections of the residues. In our earlier work [21], the responsible factors for the errors and uncertainties are described in detail. The spectroscopic properties like half-lives, characteristic γ-ray energies, branching ratios, and spins of the identified ERs are taken from Refs. [50,51] and listed in Table I along with the respective residues.

TABLE I. List of identified evaporation residues produced in the interaction of ^{13}C with ^{175}Lu along with their spectroscopic properties like half-lives, characteristic γ-ray energies, branching ratios, and spins.

Residues	Emission channel ^{13}C + ^{175}Lu	Half-life ($T_{1/2}$)	J^π	E_γ (keV)	I_γ (%)
^{184}Ir	$4n$	3.09 h	5^-	119.80	30.3
				390.38	25.7
				961.22	12.4
^{183}Ir	$5n$	58.0 min	$5/2^-$	228.70	6.9
				282.39	4.9
				392.52	10.4
^{182}Ir	$6n$	15.0 min	3^+	127.0	35.6
				273.40	46.3
^{183g}Os	$p4n$	13.0 h	$9/2^+$	114.46	20.6
				167.84	8.8
				381.77	89.6
^{183m}Os	$p4n$	9.9 h	$1/2^-$	1101.94	49.0
				1107.92	22.4
^{182}Os	$p5n$	22.1 h	0^+	130.83	3.3
				180. 22	33.5
				263.29	6.7
^{183}Re	αn	70.0 d	$5/2^+$	162.32	23.3
^{181}Re	$\alpha 3n$	19.9 h		360.70	20.0
				365.57	56.0
^{179}Re	$\alpha 5n$	19.5 min	$5/2^+$	289.97	26.9
				430.22	28.0
^{178m}Ta	$2\alpha 2n$	2.36 h	7^-	213.44	81.4
				325.56	94.1
				426.38	97.0
^{177}Ta	$2\alpha 3n$	56.56 h	$7/2^+$	112.95	7.2
^{176}Ta	$2\alpha 4n$	8.09 h	1^-	201.83	6.0
				1159.28	25.0

III. ANALYSIS AND ESTIMATION OF THE MEASURED FRRDs

In the present paper, several ERs—^{184}Ir ($4n$), ^{183}Ir ($5n$), ^{182}Ir ($6n$), ^{183}Os ($p4n$), ^{182}Os ($p5n$), ^{183}Re (αn), ^{181}Re ($\alpha 3n$), ^{179}Re ($\alpha 5n$), ^{178m}Ta ($2\alpha 2n$), ^{177}Ta ($2\alpha 3n$), and ^{176}Ta ($2\alpha 4n$)—produced in the interaction of the projectile ^{13}C with the target ^{175}Lu, have been identified at $\approx$88-MeV energy. The present FRRD analysis of ERs is accomplished in the

framework of range-energy loss calculations based on the code SRIM [46] to justify the formation of evaporation residues via CF (full LMT) and/or ICF (partial LMT). Owing to the proportionality with the fused fragment mass, the full LMT gives the maximum recoil velocity to the CF products. The incompletely fused composite (IFC) system formed due to the partial LMT has nonunique mass, energy, and momentum values compared with the compound nucleus (CN) formed due to the CF process. Thus, the FRRD measurement is a promising way to give the direct measure of full and/or partial LMT from the projectile to the target nucleus. The degree of the LMT (ρ_{LMT}) associated with the FRRD measurement may be given as

$$\rho_{\mathrm{LMT}} = \frac{P_{\mathrm{frac}}}{P_{\mathrm{proj}}}, \tag{1}$$

where P_{frac} is the linear momentum associated with the fused part of the projectile and P_{proj} is the linear momentum for the entire projectile amalgamation with the target nucleus. The width of the velocity distribution of the ERs depends upon the particles evaporated from the equilibrated CN. The most probable velocity, v_0, may be given as

$$v_0 = v_{\mathrm{CN}} = \frac{\sqrt{2M_P E}}{M_{P+T}}, \tag{2}$$

where M_P is the mass of the projectile, M_{P+T} is the mass of the compound system (projectile + target), and E is the incident projectile energy. As linear momentum is proportional to the fused mass of the projectile, the ERs populated via the partial LMT show a smaller depth in the stopping medium than those for the entire LMT. Moreover, the various degrees of the LMT (ρ_{LMT}) from the projectile to the target may give rise to different recoil ranges in the stopping medium. Hence, the investigation of FRRDs is a well-established method to distinguish the CF and/or ICF reaction processes and also to separate out the relative contributions of different fusion components. The nonunique mass, energy, and momentum values of an incompletely fused composite system may be resulting due to the fluctuations in the fused mass from the projectile to the target nucleus and various interaction trajectories.

The measured cross section of the recoiled residues in each catcher foil was divided by the respective catcher foil thickness to estimate the normalized yields. Further, the FRRDs have been obtained by plotting the normalized yields against the cumulative catcher foil thickness. The overall errors in relative contributions are estimated to be less than 15% and the size of the circles in the FRRD figures includes the uncertainty in the yield values. The measured FRRDs disentangling the different fusion components are displayed in Figs. 1–3. The yield curves of the ERs are assumed to be Gaussian in nature and fitted with a Gaussian distribution using the software ORIGIN, which may be given as

$$Y = Y_0 + \frac{A}{\omega_A\sqrt{2\pi}} e^{-(R-R_P)^2/2\pi\omega_A^2}, \tag{3}$$

where R_P is the most probable mean recoil range,ω_A is the width parameter [full width at half maximum (FWHM)] of distribution, and A is the area associated with the respective peak. The normalized yield Y may be estimated by the chi-square (χ^2) fit of the experimentally measured FRRDs and may be represented as

$$\chi^2 = \frac{1}{(m-p-1)}\,[Y(A) - Y_0(A)]^2. \tag{4}$$

The χ^2 value was minimized in the present paper by using a nonlinear least-square fit routine, keeping the width parameter (ω_A) and the most probable mean recoil range (R_P) as free parameters. In the case of αxn and $2\alpha xn$ emission channels, the experimentally measured FRRDs have been fitted by using the multipeak option in ORIGIN software.

As already mentioned, the measured FRRDs of ERs are examined in the framework of the code SRIM to confirm the formation of residues via CF and/or ICF. The code SRIM is a group of programs, which calculates interaction of ions with the matter. The programs were developed by Ziegler *et al.* [52,53]. The theoretical treatment of the stopping of ions in matter is in large measure due to the work of Bohr [54], Bethe [55], Bloch [56], and Lindhard *et al.* [57], among others. The stopping power depends on the ion's charge and its velocity. The Bohr velocity (v_0) is expressed as 25 keV/amu, which is basically the velocity of the conduction electrons in a solid. Ions with velocities below v_0 have adiabatic collisions with target electrons and hence small stopping powers. The stopping power increases with increasing ion velocity until a peak occurs at about $v_{\mathrm{peak}} = 3v_0 z_1^{2/3}$ where z_1 is the ion atomic number. At velocities above the stopping peak, the strength of the interaction between an ion and a target electron saturates and the duration of any interaction becomes shorter. Thus, the stopping power decreases with increasing ion velocity. Since, the maximum ion-target interaction occurs at the stopping peak, this is the region which should have the greatest deviation from Bragg's rule. The energy loss of ions in matter passing through the matter could be divided into two components: nuclear stopping power (energy loss to the medium's atomic positive cores) and electronic stopping power (energy loss to the medium's light electrons). The electronic stopping power was observed to be far greater than the nuclear stopping power for energetic light ions.

A major advance in the understanding of stopping power took place later when Bethe [55] and Bloch [56] restated the problems from the perspective of quantum mechanics. SRIM produces the tables of stopping powers, ranges, and straggling distributions for any ion at any energy in any elemental target. More elaborate calculations include targets with complex multilayer configurations. This code is basically based on the Monte Carlo simulation method, namely, the binary collision approximation with a random selection of the impact parameter of the next colliding ion. It needs the ion type and energy (in the range 10 eV–2GeV) and the material of one or several target layers. The breakup fusion model [16] of ICF is used for the theoretical calculations of excitation energy of the intermediate compound system, needed for SRIM calculation.

The theoretical mean recoil ranges (R_P^{theo}) of ERs produced via CF of the projectile ^{12}C with the target to form CN have been calculated using the code SRIM. As displayed

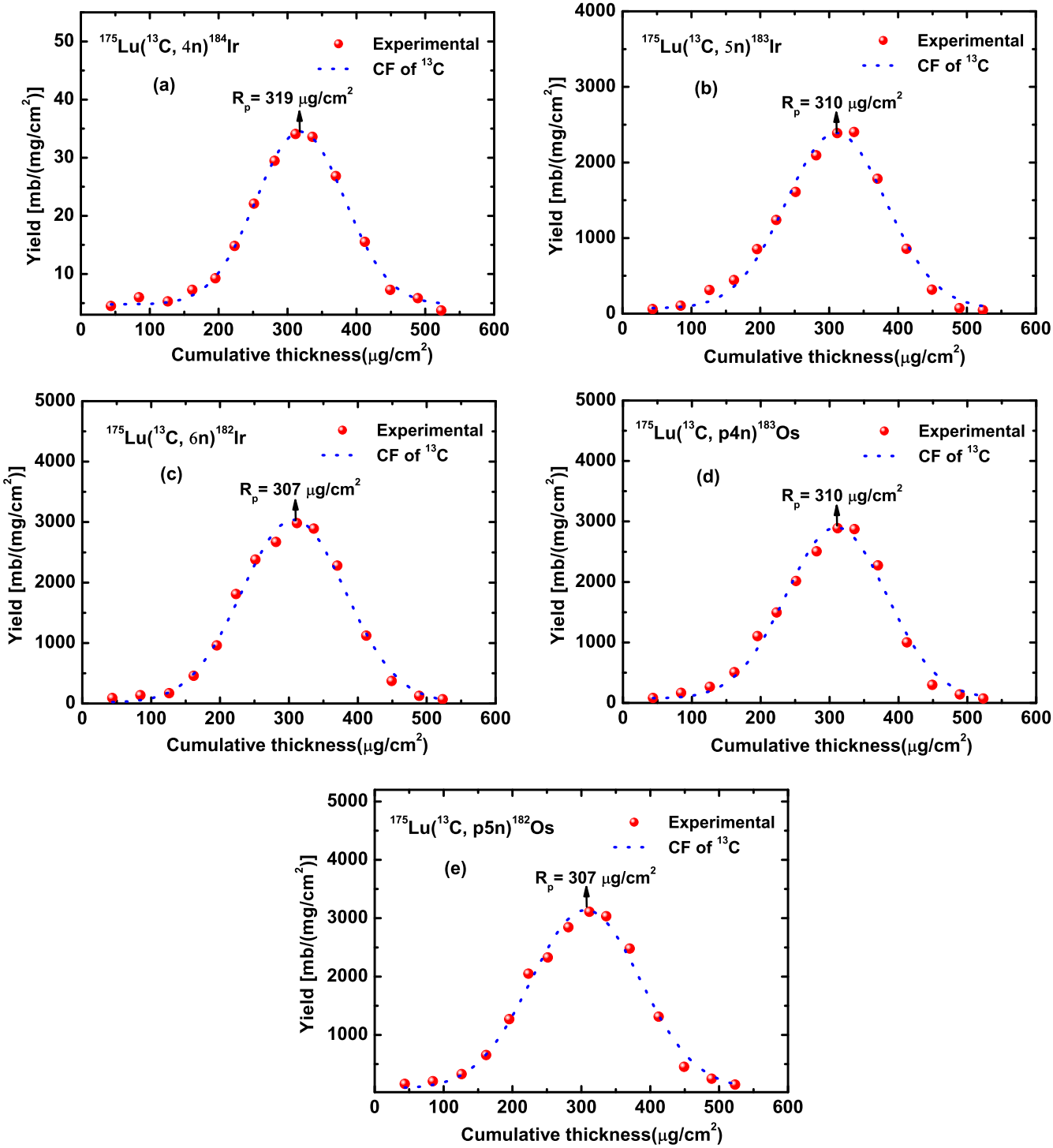

FIG. 1. Experimentally measured FRRDs for the residues (a) ^{184}Ir ($4n$), (b) ^{183}Ir ($5n$), (c) ^{182}Ir ($6n$), (d) ^{183}Os ($p4n$), and (e) ^{182}Os ($p5n$) populated in the ^{13}C + ^{175}Lu system.

in Figs. 1(a)–1(e), the residues ^{184}Ir ($4n$), ^{183}Ir ($5n$), ^{182}Ir ($6n$), ^{183}Os ($p4n$), and ^{182}Os ($p5n$) formed via xn and pxn channels are observed to show a single Gaussian peak in their respective FRRDs. The exhibition of only one peak in the distribution pattern, indicates the involvement of a single LMT component in the population of these residues. The observed ranges $R_P^{\text{exp}} \approx 319$, ≈ 310, ≈ 307, ≈ 310, and ≈ 307 μg/cm^2 for the residues ^{184}Ir ($4n$), ^{183}Ir ($5n$), ^{182}Ir ($6n$), ^{183}Os ($p4n$), and ^{182}Os ($p5n$), respectively, well match with the theoretical range $R_P^{\text{theo}} \approx 327$ μg/cm^2 calculated for the CN ^{188}Ir* (formed due to the fusion of ^{13}C with target ^{175}Lu) using the code SRIM. The close agreement between measured

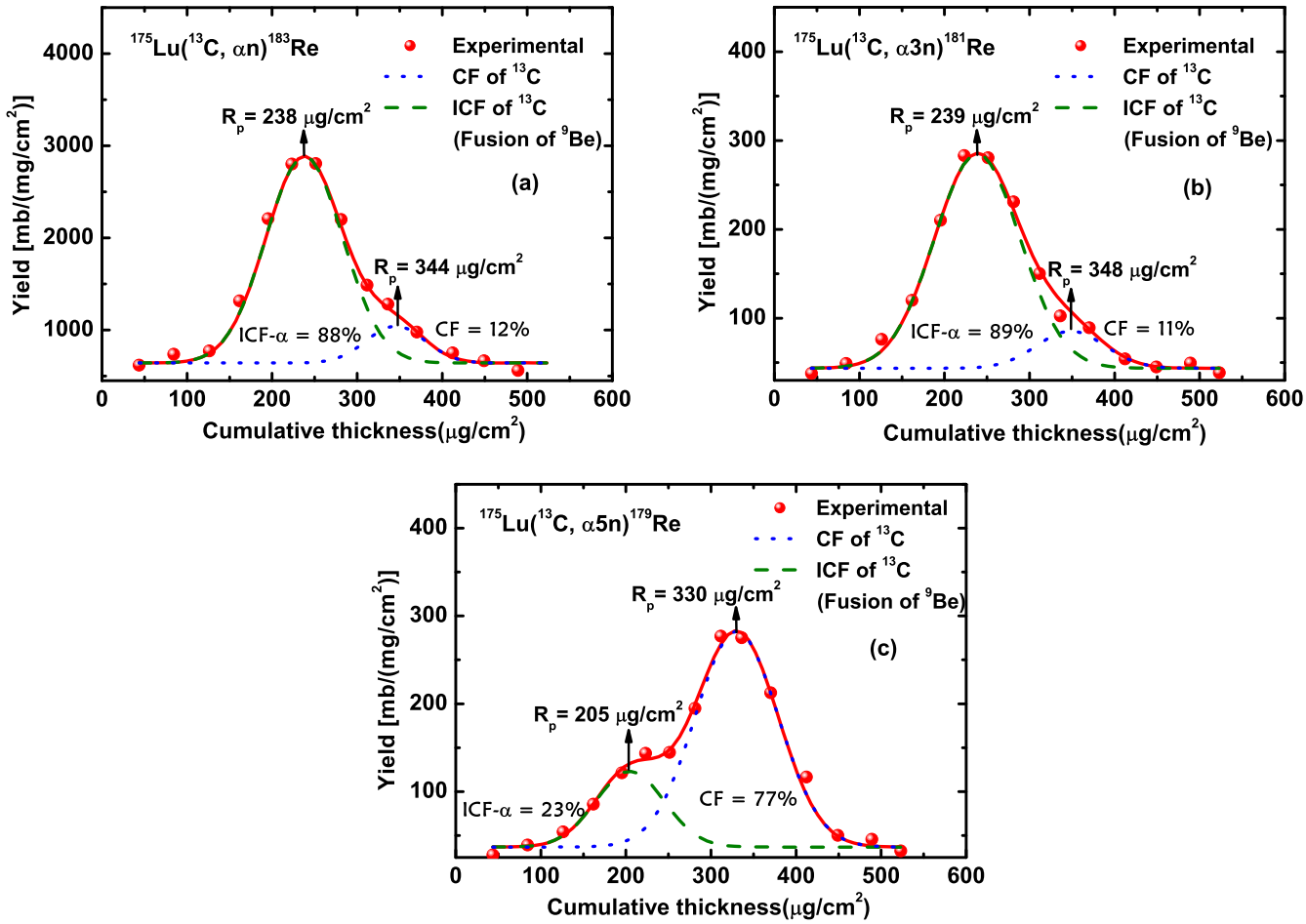

FIG. 2. Experimentally measured FRRDs for the residues (a) ^{183}Re (αn), (b) ^{181}Re ($\alpha 3n$), and (c) ^{179}Re ($\alpha 5n$) populated in the ^{13}C + ^{175}Lu system.

and theoretical recoil ranges indicates the population of these residues via the entire LMT from the projectile to the target, i.e., via CF process. Moreover, the equilibrated CN ^{188}Ir* may decay via the statistical emission of four, five, and six neutrons, respectively, to form ^{184}Ir, ^{183}Ir, and ^{182}Ir and the emission of one proton along with four and five neutrons, respectively, to form the residues ^{183}Os ($p4n$) and ^{182}Os ($p5n$). The most probable mean recoil ranges ($R_P^{\rm exp}$) deduced from the measured FRRD curves and theoretically calculated mean recoil ranges ($R_P^{\rm theo}$) for the ERs produced via CF (full LMT) and/or ICF (partial LMT) components in the ^{13}C + ^{175}Lu system are given in Table II. The reaction mechanism involved in the case of *xn*-*pxn* channels may be represented as

$$^{13}\mathrm{C} + {}^{175}\mathrm{Lu} \rightarrow {}^{188}\mathrm{Ir}^* \rightarrow {}^{188-x}\mathrm{Ir} + xn \quad (x = 4,\ 5,\ 6),$$

$$^{13}\mathrm{C} + {}^{175}\mathrm{Lu} \rightarrow {}^{188}\mathrm{Ir}^* \rightarrow {}^{187-x}\mathrm{Os} + pxn \quad (x = 4,\ 5).$$

In Figs. 2(a)–2(c), the observed FRRDs of αxn emission channel residues ^{183}Re (αn), ^{181}Re ($\alpha 3n$), and ^{179}Re ($\alpha 5n$) are displayed and fitted into the multipeak composite shape using the ORIGIN software. The presence of two clearly resolved differently ranged Gaussian peaks gives the signature of the fusion of another component in addition to ^{13}C with the target. These αxn emission channel residues are expected to be produced via both CF and/or ICF processes. As a representative case, the FRRD of residue ^{183}Re (αn) is represented in Fig. 2(a). As shown in this figure, the measured FRRD is resolved into two Gaussian peaks at cumulative depth ≈344 and ≈238 μg/cm^2, respectively. The peak at larger cumulative thickness ≈344 μg/cm^2 indicates the full LMT of projectile ^{13}C to the target ^{175}Lu; however, the second peak at comparatively smaller cumulative thickness ≈238 μg/cm^2 indicates the fusion of ^{9}Be with the target (if ^{13}C is assumed to break up into ^{9}Be + α), respectively. Both observed recoil ranges ($R_P^{\rm exp}$) match well with $R_P^{\rm theo}$ (≈327 μg/cm^2 for ^{13}C fusion and ≈229 μg/cm^2 for ^{9}Be fusion) calculated using the code SRIM. It may be pointed out from this figure that the fusion of ^{9}Be with the target also contributes significantly along with CF in the population of this residue. Similarly, the measured FRRDs of ERs ^{181}Re ($\alpha 3n$) and ^{179}Re ($\alpha 5n$) also show two well-resolved Gaussian peaks as displayed in Figs. 2(b) and 3(c). These figures also exhibit the presence of another fusion component (^{9}Be) in addition to the ^{13}C, and in turn the contribution from the ICF along with the CF. The measured most probable mean recoil ranges ($R_P^{\rm exp}$) along with the theoretically calculated mean recoil ranges ($R_P^{\rm theo}$) for the ERs produced via CF and/or ICF components in the ^{13}C + ^{175}Lu system are given in Table II. The reaction

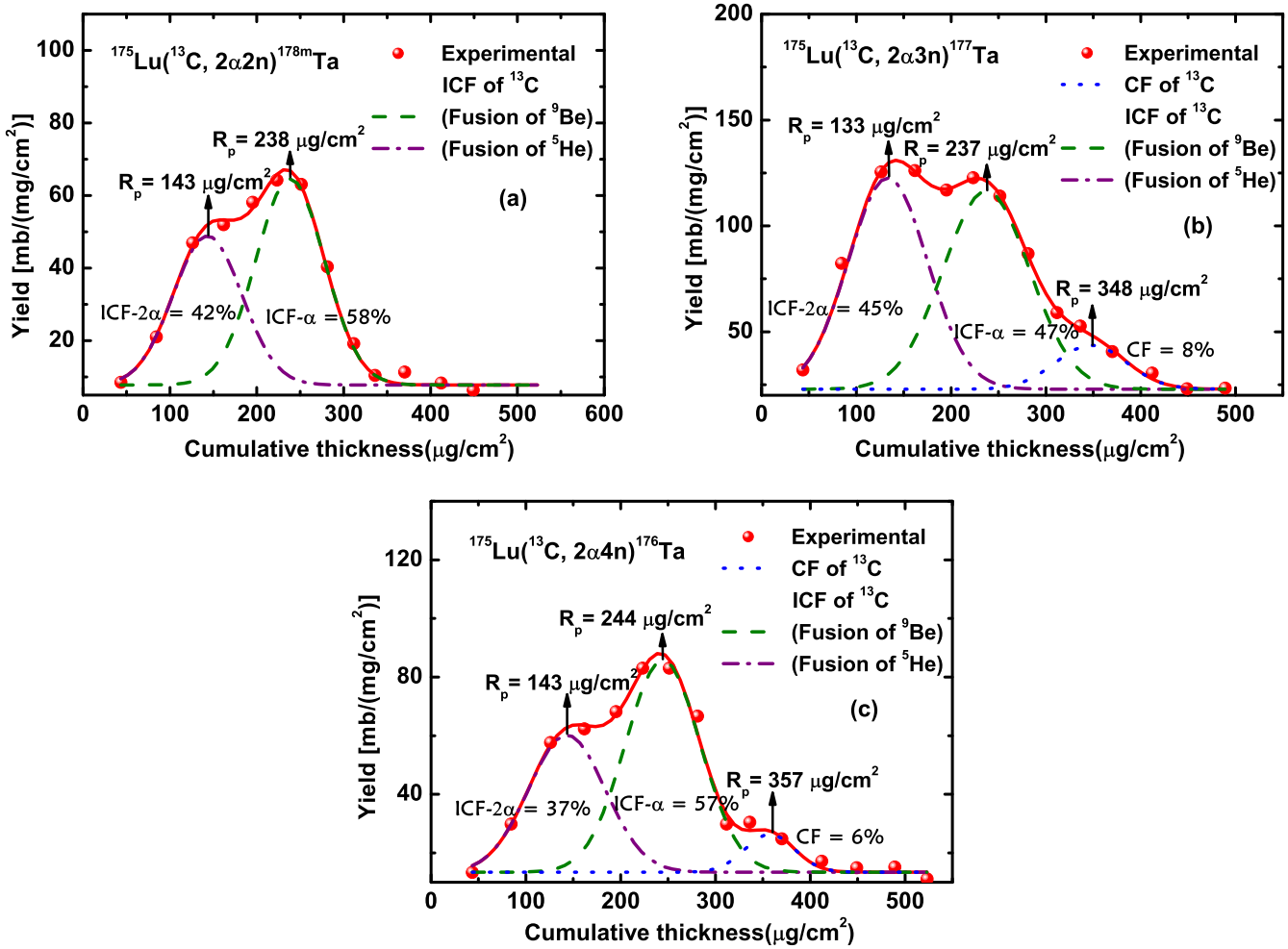

FIG. 3. Experimentally measured FRRDs for the residues (a) ^{178m}Ta ($2\alpha 2n$), (b) ^{177}Ta ($2\alpha 3n$), and (c) ^{176}Ta ($2\alpha 4n$) populated in the ^{13}C + ^{175}Lu system.

mechanism involved in the case of the αxn emission channel may be represented as (i) the CF of the projectile ^{13}C,

$$^{13}\mathrm{C} + {}^{175}\mathrm{Lu} \rightarrow {}^{188}\mathrm{Ir}^* \rightarrow {}^{184-x}\mathrm{Re} + \alpha xn \quad (x = 1,\ 3,\ 5),$$

and (ii) the ICF of the projectile ^{13}C (fusion of fragment ^{9}Be),

$$^{13}\mathrm{C}(^{9}\mathrm{Be} + \alpha) + {}^{175}\mathrm{Lu} \rightarrow {}^{184}\mathrm{Re}^* \rightarrow {}^{184-x}\mathrm{Re} + xn \quad (x = 1,\ 3,\ 5),$$

where α moves as a spectator.

Further, the measured FRRDs of the residues ^{178m}Ta ($2\alpha 2n$), ^{177}Ta ($2\alpha 3n$), and ^{176}Ta ($2\alpha 4n$) also show well-resolved multi-Gaussian peaks, displayed in Figs. 3(a)–3(c). In the case of residue ^{178m}Ta ($2\alpha 2n$), two Gaussian peaks are observed at cumulative thicknesses ≈221 and ≈121 μg/cm^2, respectively. Both observed recoil ranges match well with $R_P^{\mathrm{theo}} \approx 229$ and ≈145 μg/cm^2, respectively, calculated using the code SRIM for the IFC systems ^{184}Re* (formed due to the fusion of ^{9}Be) and ^{180}Ta* (formed due to the fusion of α). It is worth mentioning that the absence of the larger range peak associated with the CF thickness is attributed to the population of residue ^{178m}Ta via ICF process only. On the other hand, the measured FRRDs of the residues ^{177}Ta ($2\alpha 3n$) and ^{176}Ta ($2\alpha 4n$) are well resolved into three Gaussian peaks as shown in Figs. 3(b) and 3(c). The presence of three peaks shows clearly that fusion of fragments ^{9}Be and ^{5}He with the target (formed in the breakup of ^{13}C) also contributes significantly along with the CF process (fusion of ^{13}C). Moreover, the ICF process also plays an important role in the population of residues ^{177}Ta ($2\alpha 3n$) and ^{176}Ta ($2\alpha 4n$). The observed recoil ranges R_P^{exp} along with the theoretical recoil ranges R_P^{theo} for these residues are given in Table II. The reaction mechanism involved in $2\alpha xn$ emission channels may be represented as (i) the CF of projectile ^{13}C,

$$^{13}\mathrm{C} + {}^{175}\mathrm{Lu} \rightarrow {}^{188}\mathrm{Ir}^* \rightarrow {}^{180-x}\mathrm{Ta} + 2\alpha xn \quad (x = 2 - 4);$$

(ii) the ICF of the projectile ^{13}C (fusion of fragment ^{9}Be),

$$^{13}\mathrm{C}(^{9}\mathrm{Be} + \alpha) + {}^{175}\mathrm{Lu} \rightarrow {}^{184}\mathrm{Re}^* \rightarrow {}^{180-x}\mathrm{Ta} + \alpha xn \quad (x = 2 - 4),$$

where α moves as a spectator; and (iii) the ICF of the projectile ^{13}C (fusion of fragment ^{5}He),

$$^{13}\mathrm{C}(^{5}\mathrm{He} + {}^{8}\mathrm{Be}) + {}^{175}\mathrm{Lu} \rightarrow {}^{180}\mathrm{Ta}^* \rightarrow {}^{180-x}\mathrm{Ta} + xn \quad (x = 2 - 4),$$

where ^{8}Be moves as a spectator.

TABLE II. Most probable mean ranges ($R_P^{\rm exp}$) deduced from experimentally measured FRRDs and theoretically estimated mean recoil ranges ($R_P^{\rm theo}$) in units of μg/cm^2 for residues produced via CF (entire LMT) and/or ICF (fractional LMT) in the interaction of ^{13}C with ^{175}Lu at ≈88-MeV energy.

Residues	CF of ^{13}C		ICF of ^{13}C			
			Fusion of ^{9}Be		Fusion of ^{5}He	
	$R_P^{\rm exp}$	$R_P^{\rm theo}$	$R_P^{\rm exp}$	$R_P^{\rm theo}$	$R_P^{\rm exp}$	$R_P^{\rm theo}$
^{184}Ir ($4n$)	319 ± 65	327				
^{183}Ir ($5n$)	310 ± 72	327				
^{182}Ir ($6n$)	307 ± 75	327				
^{183}Os ($p4n$)	310 ± 73	327				
^{182}Os ($p5n$)	307 ± 79	327				
^{183}Re (αn)	344 ± 35	327	238 ± 45	229		
^{181}Re ($\alpha 3n$)	348 ± 40	327	239 ± 50	229		
^{179}Re ($\alpha 5n$)	330 ± 49	327	205 ± 41	229		
^{178m}Ta ($2\alpha 2n$)		327	238 ± 39	229	143 ± 39	145
^{177}Ta ($2\alpha 3n$)	348 ± 38	327	237 ± 45	229	133 ± 42	145
^{176}Ta ($2\alpha 4n$)	357 ± 26	327	244 ± 39	229	143 ± 40	145

In the case of αxn and $2\alpha xn$ emission channels, the relative contributions for the individual fusion components, i.e., ^{13}C, ^{9}Be, and ^{5}He, have also been separated out from the present analysis. They are obtained by dividing the area under the peak of the corresponding fusion component by the total area associated with the FRRD of the respective residue. In Table III, the deduced relative contributions due to the different fusion components in the population of residues ^{184,183,182}Ir, ^{183,182}Os, ^{183,181,179}Re, and ^{178m,177,176}Ta are given. The contributions coming from the fusion components ^{13}C and/or ^{9}Be and/or ^{5}He are also shown in the respective FRRDs (Figs. 2 and 3). It may also be seen from the present FRRD analysis that the projectile ^{13}C may break up into its fragments ^{9}Be-^{4}He(α) and/or ^{5}He-^{8}Be (2α) near the target nuclear field, following the basic assumption of the breakup fusion model. Moreover, these αxn and $2\alpha xn$ emission channel residues

TABLE III. Measured relative contribution of CF and/or ICF components obtained from experimentally measured FRRDs of residues produced in the interaction of ^{13}C with ^{175}Lu at ≈88-MeV energy.

Residues	CF of ^{13}C	ICF of ^{13}C	
	(%)	Fusion of ^{9}Be (%)	Fusion of ^{5}He (%)
^{184}Ir ($4n$)	100		
^{183}Ir ($5n$)	100		
^{182}Ir ($6n$)	100		
^{183}Os ($p4n$)	100		
^{182}Os ($p5n$)	100		
^{183}Re (αn)	12	88	
^{181}Re ($\alpha 3n$)	11	89	
^{179}Re ($\alpha 5n$)	77	23	
^{178m}Ta ($2\alpha n$)		58	42
^{177}Ta ($2\alpha 2n$)	8	47	45
^{176}Ta ($2\alpha 3n$)	6	57	37

TABLE IV. The normalized peak width (FWHM/$R_P^{\rm exp}$) deduced from the measured FRRDs of residues produced via CF (full LMT) and/or ICF (partial LMT) components in the interaction of ^{13}C with ^{175}Lu at ≈88 MeV.

Residues	CF of ^{13}C	ICF of ^{13}C	
		Fusion of ^{9}Be	Fusion of ^{5}He
^{184}Ir ($4n$)	0.41 ± 0.08		
^{183}Ir ($5n$)	0.46 ± 0.11		
^{182}Ir ($6n$)	0.48 ± 0.12		
^{183}Os ($p4n$)	0.47 ± 0.11		
^{182}Os ($p5n$)	0.51 ± 0.13		
^{183}Re (αn)	0.20 ± 0.02	0.38 ± 0.07	
^{181}Re ($\alpha 3n$)	0.23 ± 0.03	0.42 ± 0.09	
^{179}Re ($\alpha 5n$)	0.30 ± 0.04	0.40 ± 0.08	
^{178m}Ta ($2\alpha n$)		0.33 ± 0.05	0.55 ± 0.15
^{177}Ta ($2\alpha 2n$)	0.22 ± 0.02	0.38 ± 0.07	0.63 ± 0.19
^{176}Ta ($2\alpha 3n$)	0.15 ± 0.01	0.32 ± 0.05	0.56 ± 0.16

are also populated via ICF along with CF as expected. It is also worth mentioning that the energy and momentum of the final residues may change due to the emission of nucleons from the recoiling products. Such perturbing effect on the recoil velocity of the ERs is reflected in the peak width (FWHM) of the measured FRRDs. The width may also arise due to the contribution from the straggling effects. An attempt has also been toward consistency in the peak width (FWHM) of measured FRRDs of ERs produced via CF and/or ICF processes. The deduced normalized peak widths (FWHM/$R_P^{\rm exp}$) are tabulated in Table IV. The normalized peak width values are found consistent for the CF and the ICF residues individually. In the case of αxn and $2\alpha xn$ emission channels, the average normalized peak width for the CF is ≈0.22; however, for ICF-α (i.e., fusion of fragment ^{9}Be) and ICF-2α (i.e., fusion of fragment ^{5}He), the average normalized peak width increases to ≈ 0.37 and 0.58, respectively, as expected.

IV. ICF CORRELATION WITH VARIOUS ENTRANCE CHANNEL PARAMETERS

As mentioned earlier, the FRRD measurement is a promising method to distinguish the CF and/or ICF processes. The FFRDs analysis makes it possible to obtain directly the relative contributions of individual fusion components in the breakup of the projectile into its fragments (^{13}C, ^{9}Be, and ^{5}He in the case of the projectile ^{13}C). In the present paper, an attempt has been made to gain better insight into the dependence of various entrance channel parameters on the ICF reaction dynamics. The ICF probability function ($F_{\rm ICF}$) has been deduced for the present ^{13}C + ^{175}Lu system and studied as a function of these parameters. The $F_{\rm ICF}$ is a measure of the strength of the ICF relative to the total fusion cross section ($\Sigma\sigma_{\rm TF} = \Sigma\sigma_{\rm CF} + \Sigma\sigma_{\rm ICF}$), and is evaluated by using the relation as

$$F_{\rm ICF} = \Sigma\sigma_{\rm ICF}/(\Sigma\sigma_{\rm CF} + \Sigma\sigma_{\rm ICF}), \quad (5)$$

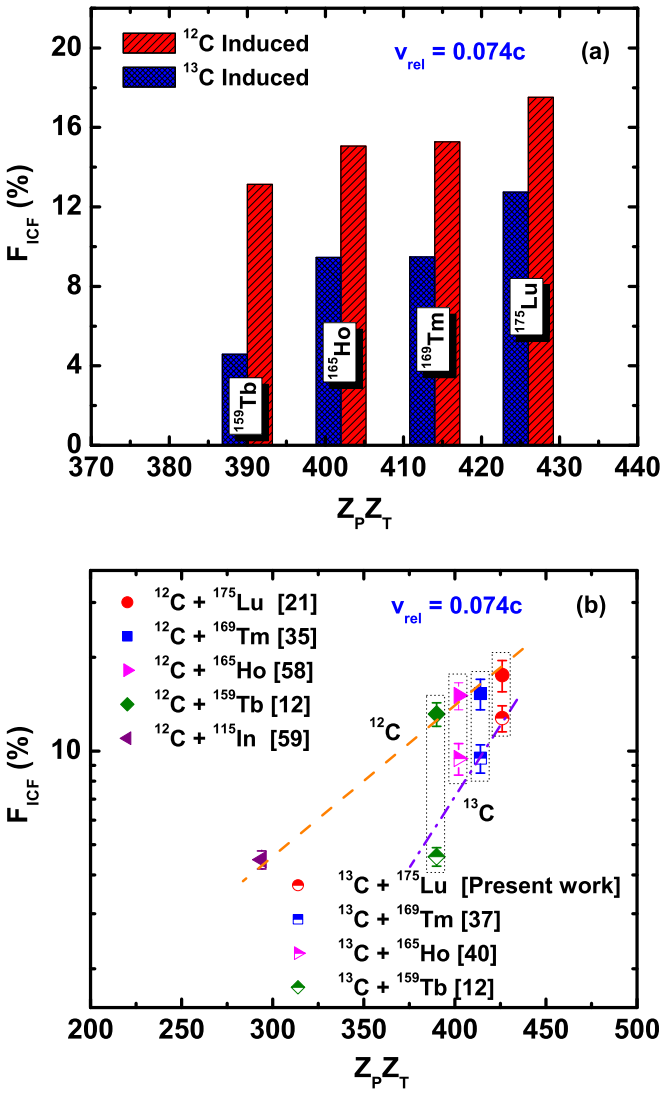

FIG. 4. The F_{ICF} (%) deduced from the present FRRD analysis along with those obtained for earlier studied systems as a function of Coulomb factor (Z_PZ_T) at the same relative velocity ($v_{rel} = 0.074c$). The color lines drawn through the data points are just to guide the eyes.

where $\Sigma\sigma_{CF}$ and $\Sigma\sigma_{ICF}$ are the sums of CF and ICF channel cross sections respectively, extracted from the present FRRD analysis.

A. ICF behavior with the Coulomb factor (Z_PZ_T)

In the present paper, an attempt has been made to understand the dependence of ICF with the product of projectile and target charges Z_PZ_T (referred to as the Coulomb factor between interacting partners) more effectively. The ICF fraction (F_{ICF}) deduced from the present FRRD analysis for the system $^{13}C + ^{175}Lu$ along with those obtained for the systems $^{12}C + ^{175}Lu$ [21], $^{12}C + ^{169}Tm$ [35], $^{12}C + ^{165}Ho$ [58], $^{12}C + ^{159}Tb$ [12], $^{12}C + ^{115}In$ [59], $^{13}C + ^{169}Tm$ [37], $^{13}C + ^{159}Tb$ [12], and $^{13}C + ^{165}Ho$ [40], available in literature, has been plotted as a function of Z_PZ_T and shown in Figs. 4(a) and 4(b). In this figure, the F_{ICF} values have been plotted at the same relative velocity ($v_{rel} = 0.074c$) to cancel out the effect of different Coulomb barriers due to the different projectile-target systems. In a recent paper, Shuaib *et al.* [39] observed a systematic linear growth in F_{ICF} with increasing the parameter Z_PZ_T. However, as shown in Figs. 4(a) and 4(b), a simple linear growth in F_{ICF} is not observed with the increase of Z_PZ_T, and is in some contradiction to the recent findings reported in Ref. [39]. As can be seen from these figures, for the systems having the same Z_PZ_T values (marked by dotted vertical boxes), the F_{ICF} values are found to be noticeably different. It may also be pointed out from Fig. 4(b) that the F_{ICF} values deduced for the projectiles ^{12}C and ^{13}C follow a linear trend with increasing the parameter Z_PZ_T, but separately for each projectile. Lower F_{ICF} values are observed for the reactions induced by ^{13}C than for ^{12}C with the targets of the same Z_T. The present results based on Z_PZ_T dependence of ICF support well the recently observed similar findings [40,41]. Moreover, this paper shows clearly that the Coulomb factor (Z_PZ_T) affects the ICF reaction dynamics but separately for different isotopes of the same projectile (having the same Z_P), i.e., ^{12}C and ^{13}C.

B. ICF behavior with the target deformation

Gerschel [42] and Singh *et al.* [11] studied the role of target deformation in ICF dynamics on the basis of the localization of the ℓ window. These observations show that the mean input angular momentum values for αxn emission channels produced via ICF are comparatively higher for the reactions induced with a more deformed target nucleus than for the less deformed or spherical nucleus. In turn, the higher projectile breakup probability is found in the case of the deformed target nucleus.

In order to understand the target deformation dependence of the ICF process in a more clear way, the deduced F_{ICF} for the present system $^{13}C + ^{175}Lu$ along with the earlier studied systems [12,21,35,37,40,58] has been plotted as a function of the target deformation parameter (β_2), and shown in Figs. 5(a) and 5(b). The β_2 values for different targets are taken from Ref. [60]. The formulation and detailed information about the β_2 parameter are given in Ref. [61]. The deformation parameter describes the shape of an axially symmetric deformed nucleus and is correlated directly to the quadruple moment. In Fig. 5(a), the F_{ICF} values deduced for the reactions induced by the projectile ^{12}C have been plotted. However, the F_{ICF} values deduced for the reactions induced by ^{13}C are represented in Fig. 5(b). As shown in these figures, the F_{ICF} does not follow any schematic trend. It is observed that the reactions with the target ^{175}Lu have the higher F_{ICF} value than those for the targets ^{165}Ho and ^{169}Tm, irrespective of ^{175}Lu having a lower β_2 value compared with ^{165}Ho and ^{169}Tm. As shown in this figure, in general the larger ICF fraction is observed for the projectile ^{12}C induced reactions than that for ^{13}C, while the β_2 parameter values are equal for the reactions induced by both projectiles with respective targets. Furthermore, this figure also reflects the projectile structure influence on the ICF process. The present findings indicate that the β_2 parameter alone is not able to explain the ICF process at low projectile energies. Some information extracted on the basis of observed

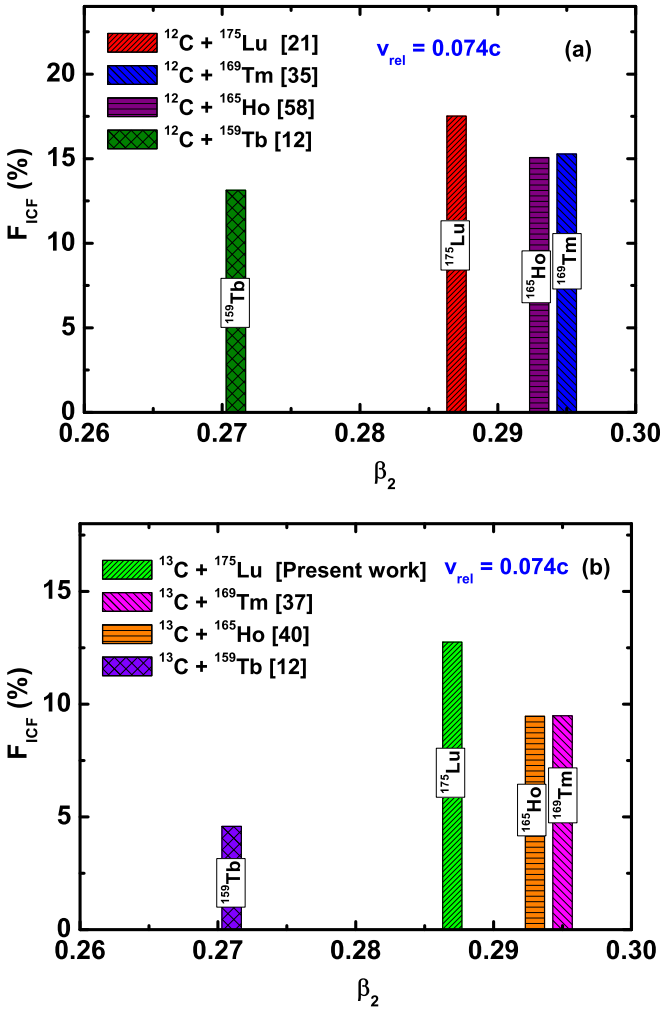

FIG. 5. The deduced F_{ICF} (%) for (a) ^{12}C induced reactions and (b) ^{13}C induced reactions as a function of target deformation parameter (β_2) at the same relative velocity ($v_{rel} = 0.074c$).

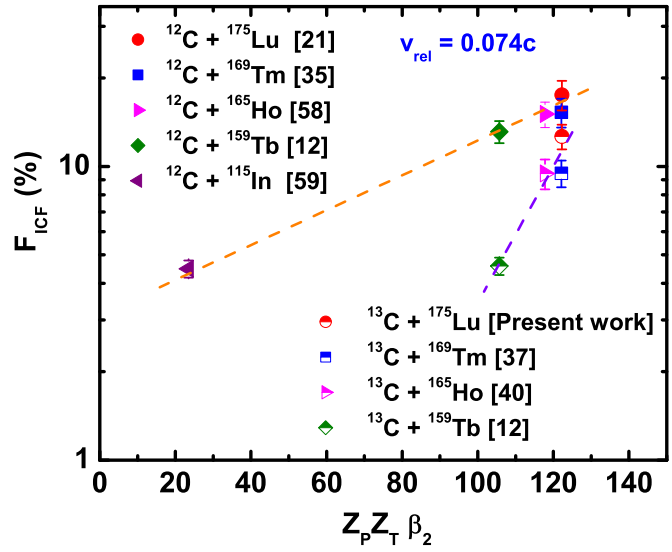

FIG. 6. The F_{ICF} (%) deduced from the present FRRD analysis along with those obtained for earlier studied systems as a function of parameter $Z_PZ_T\beta_2$. The color lines drawn through the data points are just to guide the eyes.

ICF behavior with the target deformation has been reported in recent studies [62,63].

In order to overcome the discrepancy observed in the β_2 dependence of the ICF and also to have better insight into the effect of the Coulomb factor (Z_PZ_T), in the present paper the deduced F_{ICF} has also been studied as a function of parameters $Z_PZ_T\beta_2$ and $Z_PZ_T/(1-\beta_2)$, separately. As shown in Fig. 6, the deduced F_{ICF} for the present system $^{13}C + ^{175}Lu$ along with the earlier studied systems [12,21,35,37,40,58,59] has been plotted as a function of parameter $Z_PZ_T\beta_2$ at the same relative velocity ($v_{rel} = 0.074c$). The linear growth in F_{ICF} with increasing the parameter $Z_PZ_T\beta_2$ is observed to be different for the projectile ^{12}C and ^{13}C induced reactions and the present findings based on this parameter are found in good agreement with our recent observations [41]. It may be pointed out that the ICF dependence with parameter $Z_PZ_T\beta_2$ may be explained only for the deformed target nuclei having the nonzero β_2 values. Hence, in order to incorporate the spherical along with deformed target nuclei, the deduced F_{ICF} for the present $^{13}C + ^{175}Lu$ system along with the earlier studied systems [12,21,35,37,40,58,59] has been plotted as a function of new parameter $Z_PZ_T/(1-\beta_2)$ and displayed in Fig. 7(a) at the same relative velocity ($v_{rel} = 0.074c$). As shown in this figure, the F_{ICF} values are found to increase linearly with increase in the parameter $Z_PZ_T/(1-\beta_2)$, but the growth rate of the F_{ICF} is higher for reactions induced by the projectile ^{12}C than that for ^{13}C. For better insight into the ICF dependence with parameter $Z_PZ_T/(1-\beta_2)$, the F_{ICF} values deduced for ^{12}C induced reactions with targets ^{175}Lu [21], ^{169}Tm [35], ^{165}Ho [58], ^{159}Tb [12], ^{115}In [59], and ^{103}Rh [64]; ^{13}C induced reactions with targets ^{175}Lu [21], ^{169}Tm [37], ^{165}Ho [40], and ^{159}Tb [12]; and ^{16}O induced reactions with targets ^{169}Tm [35], ^{165}Ho [65], ^{159}Tb [66], and ^{115}In [23] have been plotted in Fig. 7(b) at the same relative velocity ($v_{rel} = 0.053c$). As shown in this figure, the F_{ICF} values lie on the same line for α-cluster structured projectile (^{12}C and ^{16}O) induced reactions and are relatively larger than those for non-α-cluster structured projectile (^{13}C) induced reactions. It is worthwhile to mention that as the projectile approaches the target nucleus the strength of the Coulomb interaction increases, resulting in the breakup of the projectile into its constituent fragments. Hence, the Coulomb factor (Z_PZ_T) governs the ICF process effectively. As can be seen from Figs. 6 and 7, as the normalized Coulomb factors, i.e., $Z_PZ_T\beta_2$ and $Z_PZ_T/(1-\beta_2)$, increase, the Coulomb interaction strength also increases, resulting in more probability of projectile breakup near the target nucleus. Moreover, the parameter $Z_PZ_T/(1-\beta_2)$ may be more helpful in the understanding of the role of Coulomb factor and target deformation on ICF dynamics. A strong projectile structure dependence of ICF is also observed from these figures, which may be explored more effectively in terms of the projectile α-Q value. In order to make the present observations more effective, studies with different projectile-target combinations are required.

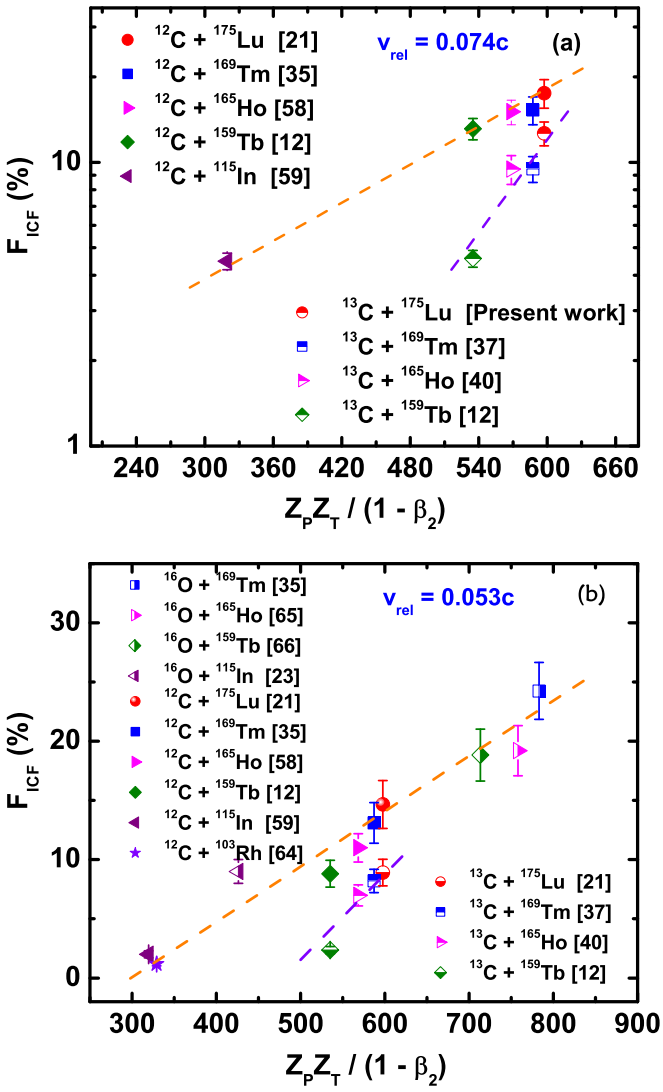

FIG. 7. The F_{ICF} (%) deduced from the present FRRD analysis along with those obtained for earlier studied systems as a function of parameter $Z_PZ_T/(1-\beta_2)$ at relative velocity (a) $v_{rel} = 0.074c$ and (b) $v_{rel} = 0.053c$. The color lines drawn through the data points are just to guide the eyes.

C. ICF behavior with the projectile α-Q value

It is noteworthy that the results represented in Figs. 4–7 and discussed on the basis of the parameters Z_PZ_T, β_2, $Z_PZ_T\beta_2$, and $Z_PZ_T/(1-\beta_2)$ indicate clearly the strong projectile structure dependence on the ICF process. In these figures, the F_{ICF} values are found comparatively higher for ^{12}C induced reactions than that for ^{13}C, irrespective of the higher binding-energy value for ^{12}C ($\approx$−7.31 MeV) than for ^{13}C ($\approx$−7.27 MeV). For the better visualization of the projectile structure effect, the F_{ICF} (%) deduced from the present FRRD analysis for the ^{13}C + ^{175}Lu system along with those obtained from the earlier excitation functions (EFs) [21] and FRRD analysis [41] have been plotted as a function of projectile α-Q value and are represented in Fig. 8. The projectile α-Q value is the energy required for the separation of the α particle from the respective projectile. As shown in

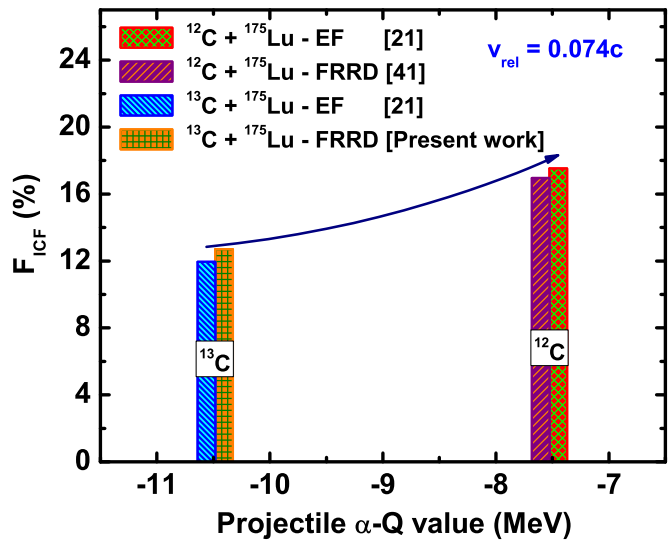

FIG. 8. The comparison of deduced F_{ICF} (%) from the present FRRD analysis along with those obtained earlier from the EF analysis (Kumar *et al.* [21]) and FRRD analysis (Kumar *et al.* [41]) at the same relative velocity ($v_{rel} = 0.074c$).

Fig. 8, a lower F_{ICF} value is observed for the more negative α-Q-value projectile ^{13}C (≈ -10.64 MeV) than for the less negative α-Q-value projectile ^{12}C (≈ -7.37 MeV). It is worth mentioning that less energy is required for the projectile ^{12}C with the lower α-Q value to break up into its α clusters than for ^{13}C. It may be inferred from the present findings that the projectile α-Q value seems to be an important entrance channel parameter in the study of ICF reaction dynamics. The present findings based on projectile α-Q-value dependence of ICF also support the recent results reported by our group [21,40,41] and others [12,23,36–38]. Further, Fig. 8 also shows good agreement between the F_{ICF} values obtained from the present FRRD data analysis and previously studied EFs data analysis [21] for the ^{12,13}C + ^{175}Lu systems and FRRD data analysis [41] for the ^{12}C + ^{175}Lu system. Hence, it may be pointed out that the results obtained in both EF and FRRD measurements are consistent with each other, which in turn strengthens the reliability of data analysis. Moreover, the present paper shows the strong projectile structure dependence of ICF by using α- and non-α-cluster projectiles with the same target. The projectile α-Q value seems to be a reliable parameter which may be responsible for the observed projectile structure effect.

D. Comparison with loosely bound projectile induced reactions

In Fig. 9, the deduced F_{ICF} (%) values for the present system and other systems induced by tightly bound projectiles (^{12}C and ^{13}C) are compared with those deduced using loosely bound projectile (^{6}Li and ^{7}Li) induced reactions (^{6}Li + ^{209}Bi [6] and ^{7}Li + ^{209}Bi [6]) and have been plotted against the parameter $Z_PZ_T/(1-\beta_2)$ at the same relative velocity ($v_{rel} = 0.074c$). As shown in this figure, no systematic trend is observed incorporating the F_{ICF} (%) values deduced for ^{6}Li and ^{7}Li induced reactions. The F_{ICF} values are found to be

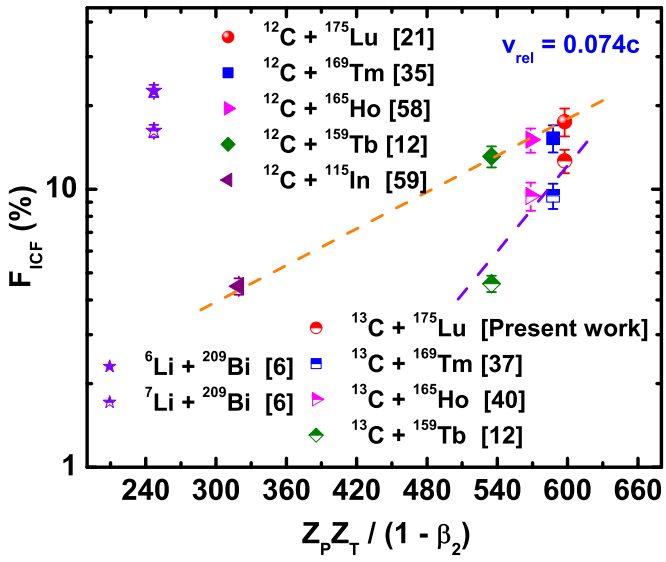

FIG. 9. The comparison between $F_{\rm ICF}$ (%) deduced using the tightly bound projectiles (^{12}C and ^{13}C) and loosely bound projectiles (^{6}Li and ^{7}Li) as a function of parameter $Z_P Z_T/(1-\beta_2)$ at relative velocity $v_{\rm rel} = 0.074c$. The color lines drawn through the data points are just to guide the eyes.

much higher for ^{6,7}Li + ^{209}Bi systems [6] than for ^{12}C and ^{13}C induced reactions. However, the $Z_P Z_T/(1-\beta_2)$ values are lower for ^{6}Li and ^{7}Li induced reactions than for ^{12}C and ^{13}C induced reactions. The alpha breakup threshold energy ($E_{\rm BU}$) of the projectile plays an important role in the fusion reaction dynamics. Higher suppression is observed for the projectiles having lower breakup threshold [6–8,43–45]. The alpha breakup threshold energy for projectiles ^{6}Li and ^{7}Li are ≈ -1.47 and ≈ -2.47 MeV, respectively, whereas the alpha breakup threshold energy for the projectiles ^{12}C and ^{13}C are ≈ -7.37 and ≈ -10.64 MeV, respectively. The projectiles ^{6}Li and ^{7}Li having lower breakup threshold energy may break up before reaching the fusion barrier, resulting in higher CF suppression at energies near and above the Coulomb barrier. Moreover, the tightly bound projectiles have higher breakup threshold energy, thereby showing less suppression compared with the loosely bound projectiles.

It is also noteworthy that the present FRRD measurement is an offline measurement method and the induced gamma-ray activities in each Al-catcher foil were recorded individually by using the HPGe detector. In this measurement, a proper range profile of thin Al-catcher foils is essential so that the different evaporation residues may trap at their respective thickness. A stream of 13–17 thin Al-catcher foils, generally, is used to make a proper range profile for the reactions induced by using the tightly bound projectiles. In the case of loosely bound projectiles like ^{6}Li, ^{7}Li, and ^{9}Be, the range calculated using the code SRIM for the entire linear momentum transfer (i.e., compound nucleus formation) is found to be much lower than that for tightly bound projectiles. For instance, in the case of ^{6,7}Li + ^{209}Bi systems [6], the calculated range for the compound nucleus (^{215,216}Rn) is only $\approx 70\,\mu$g/cm^2. In order to have the proper range profile for these systems, the average thickness for each Al foil needs to be $\approx 4-5\,\mu$g/cm^2, which is practically difficult to make. It is quite impossible to handle such thin catcher foils in air. Hence, the FRRD measurements using loosely bound projectiles like ^{6}Li, ^{7}Li, and ^{9}Be have not been carried out so far to the best of our knowledge. Moreover, due to the difficulties mentioned above for the proper range profile extraction, the direct measurements of CF and ICF cross sections for ^{6,7}Li and ^{9}Be projectiles using this method may not be possible.

E. Observation of ICF below critical angular momentum ($\ell_{\rm crit}$)

The input angular momentum (ℓ) plays a crucial role in the study of ICF reaction dynamics. As per the sharp cutoff approximation of the SUMRULE model [17], the ICF probability is assumed to exist for $\ell > \ell_{\rm crit}$ and to be zero for $\ell \leqslant \ell_{\rm crit}$. In order to have the better insight into the fusion ℓ distribution, the maximum angular momentum ($\ell_{\rm max}$) and the critical angular momentum ($\ell_{\rm crit}$) values have been calculated for the system ^{13}C + ^{175}Lu and also for the system ^{12}C + ^{175}Lu [41]. The "$\ell_{\rm max}$" is a maximum limit of angular momentum (ℓ) for which fusion may occur. The $\ell_{\rm crit}$ values calculated for the systems ^{12,13}C + ^{175}Lu by using the SUMRULE model formalism [17] are found to be 48 $\hbar$ and 50 $\hbar$, respectively. The $\ell_{\rm max}$ values are calculated by using the CCFULL code [67]. This code calculates the fusion cross sections and mean angular momentum of the compound nucleus under the influence of couplings between the relative motion and several nuclear collective motions. It takes into account the effects of nonlinear couplings to all orders, which are found to play an important role in heavy-ion fusion reactions. To make a sensible coupled-channel calculation, it is important choose a proper set of potential parameters. Potentials used for the coupled-channel calculations are of Woods-Saxon form with the following parameters: potential depth (V_0), diffuseness parameter (a_0), surface tension parameter (γ), projectile radius (R_P), and target radius (R_T). The potential depth and other parameters are calculated using Akyuz-Winther parametrization [68]. The excitation energy of the first 2^+ state in the ground rotational band, quadrupole (β_2), and hexadecapole (β_4) deformation parameters are taken from Ref. [60]. The CCFULL code includes the pair transfer coupling between the ground states and uses the macroscopic form factor given as

$$F(r) = F_t \frac{dV_N^{(0)}}{dr}, \tag{5}$$

where F_t is the coupling strength. The $\ell_{\rm max}$ values calculated by using the CCFULL code [67] are estimated as 41 $\hbar$ and 44 $\hbar$, respectively, at $\approx$88-MeV energy. In these calculations, the collective excitations of the colliding nuclei have also been taken into account. The fusion ℓ distributions for the ^{12,13}C + ^{175}Lu systems calculated by using the CCFULL code and also incorporating the coupled-channel calculations at $\approx$88-MeV energy are displayed in Fig. 10. This figure shows clearly that the $\ell_{\rm max}$ values are less than the $\ell_{\rm crit}$ values at the studied energy. The present observations indicate that $\ell_{\rm max}$ values for both the systems are not higher than that of $\ell_{\rm crit}$ for fusion at the studied energy. However, a significant ICF contribution has been obtained from the present FRRD

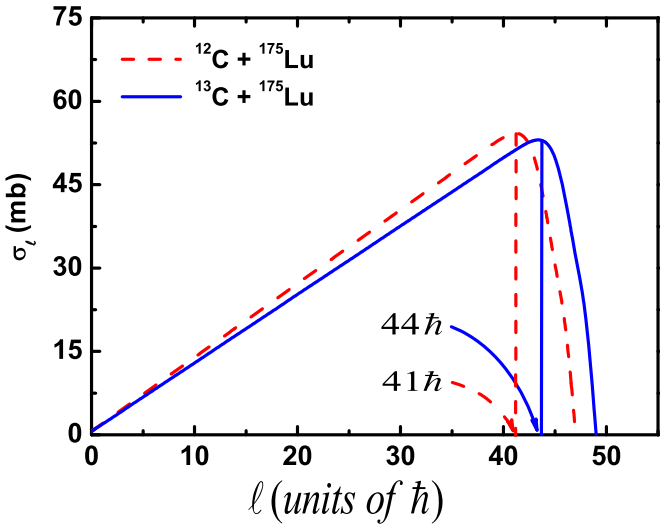

FIG. 10. Fusion ℓ distributions for the $^{12}C + ^{175}Lu$ and $^{13}C + ^{175}Lu$ systems calculated using the CCFULL code [67] and by incorporating the coupled-channel calculations at ≈88-MeV energy.

analysis as well as earlier EF analysis for the $^{12}C + ^{175}Lu$ system [41] at this energy. The present results clearly indicate that the fusion ℓ distribution window suggested in the SUMRULE model [17] is a broad diffused boundary. As such, a number of collision trajectories having values $\ell \leqslant \ell_{crit}$ may contribute significantly to the ICF. The present findings based on ICF occurrence below the ℓ_{crit} window, i.e., $\ell \leqslant \ell_{crit}$, have also been claimed in recent observations [12,13,21–23]. This paper also indicates that a refinement in the basic assumption of the SUMRULE model is needed at low projectile energies.

V. CONCLUSIONS

For better understanding of the effect of various entrance channel parameters on ICF, the FRRDs of several ERs produced in the $^{13}C + ^{175}Lu$ system have been measured at ≈88-MeV energy. The present FRRD analysis is accomplished in the framework of the code SRIM. It is observed that following the fractional LMT the ICF products traverse relatively a shorter depth in the stopping medium compared with the CF products. The basic assumption of the breakup fusion model is followed, i.e., the projectile may breakup into its fragments [presently the projectile ^{13}C breaks up into its fragments ^{9}Be-^{4}He (α) and/or ^{5}He-^{8}Be (2α)] near the target nuclear field. Presently, the relative contribution of individual fusion components, i.e., ^{13}C, ^{9}Be, and ^{5}He, has also been separated out. The ICF fraction (F_{ICF}) has also been deduced from the present analysis and compared with those obtained for the systems available in the literature to study the ICF behavior with various entrance channel parameters. It is found that the Coulomb factor (Z_PZ_T) dependence of ICF is somehow a projectile structure dependent systematic and the present results support recent observations [40,41]. From the target deformation parameter (β_2) dependent study of ICF, it is observed that as such the F_{ICF} does not follow any systematic trend. An attempt has also been made to overcome the discrepancy observed in the target deformation parameter (β_2) dependence of ICF. The F_{ICF} values are found to increase linearly with increasing the parameters $Z_PZ_T\beta_2$ and $Z_PZ_T/(1-\beta_2)$, but the growth rate is higher for the α-cluster structured projectile (^{12}C and ^{16}O) than for the non-α-cluster structured projectile (^{13}C). The parameter $Z_PZ_T/(1-\beta_2)$ may be considered an important parameter for the better understanding of the Coulomb factor and target deformation role on ICF. It may be pointed out that the projectile α-Q value is able to explain clearly the trend observed in the Z_PZ_T, β_2, $Z_PZ_T\beta_2$, and $Z_PZ_T/(1-\beta_2)$ parameter dependent study of ICF for the same values of these parameters. Presently, a lower F_{ICF} value is obtained for the projectile ^{13}C with more negative α-Q value than for ^{12}C with less negative α-Q value, and these findings support well recent observations [12,21,23,37,38]. Moreover, the projectile α-Q value seems to be an important parameter in the ICF study, which may be responsible for the observed projectile structure effect. The present FRRD analysis is also found consistent with the earlier studied EF analysis [21]. It is also observed that, having the higher alpha breakup threshold energy, the tightly bound projectiles show less CF suppression compared with the loosely bound projectiles.

Furthermore, the ICF occurrence at $\ell \leqslant \ell_{crit}$ suggests that a refinement in the basic assumption of the SUMRULE model is needed at low incident energies and more experimental data sets are required to have better insight into the fusion ℓ distribution. The present paper suggests that any single entrance channel parameter like Z_PZ_T, β_2, $Z_PZ_T\beta_2$, or $Z_PZ_T/(1-\beta_2)$ or projectile α-Q value alone is not able to explain completely the ICF process at low incident energies. Moreover, the combination of these parameters may incorporate the total features of ICF rather than a single one. As such, to have a proper visualization of low-energy ICF dynamics on various entrances channel parameters, more data sets having the same values of Z_PZ_T or β_2 or the same compound nucleus over a wide range are needed. As such, keeping in view the recent aspects, a series of refined experiments with different projectile-target combinations is planned to provide fruitful information about ICF. This study may also be helpful in the development of a proper theoretical model of ICF process at low incident energies.

ACKNOWLEDGMENTS

The authors are thankful to the Director, IUAC, New Delhi and also the Chairperson, Department of Physics, Aligarh Muslim University, Aligarh, India for providing all the necessary facilities during the experiment and data analysis. The authors are also grateful to the IUAC Target Laboratory and Pelletron technical staff for their kind support during the experiment. We are also thankful to Dr. Md. Moin Shaikh, Research Associate, Saha Institute of Nuclear Physics, Kolkata (India) for valuable discussions related to this paper. H.K. expresses his profound thanks to UGC-DAE-CSR-KC (IN) for a Fellowship under Research Project No. UGC-DAE-CSR-KC/CRS/13/NP01 sanctioned to M.A.A. The project principal investigator (M.A.A.) is also thankful to the above-mentioned funding agency for providing financial support.

[1] M. Crippa, E. Gadioli, P. Vergani, G. Ciavola, C. Marchetta, and M. Bonardi, Z. Phys. A **350**, 121 (1994).

[2] D. J. Parker, J. J. Hogan, and J. Asher, Phys. Rev. C **39**, 2256 (1989).

[3] P. Vergani, E. Gadioli, E. Vaciago, E. Fabrici, E. Gadioli Erba, M. Galmarini, G. Ciavola, and C. Marchetta, Phys. Rev. C **48**, 1815 (1993).

[4] B. S. Tomar, A. Goswami, A. V. R. Reddy, S. K. Das, P. P. Burte, S. B. Manohar, and Bency John, Phys. Rev. C **49**, 941 (1994); **58**, 3478 (1998).

[5] E. Z. Buthelezi, E. Gadioli, G. F. Steyn, F. Albertini, C. Birattari, M. Cavinato, F. Cerutti, S. H. Connell, A. A. Cowley, E. Fabrici, and E. Gadioli Erba, Nucl. Phys. A **734**, 553 (2004).

[6] M. Dasgupta, P. R. S. Gomes, D. J. Hinde, S. B. Moraes, R. M. Anjos, A. C. Berriman, R. D. Butt, N. Carlin, J. Lubian, C. R. Morton, J. O. Newton, and A. Szanto de Toledo, Phys. Rev. C **70**, 024606 (2004).

[7] P. R. S. Gomes, I. Padron, E. Crema, O. A. Capurro, J. O. Fernandez Niello, A. Arazi, G. V. Marti, J. Lubian, M. Trotta, A. J. Pacheco, J. E. Testoni, M. D. Rodriguez, M. E. Ortega, L. C. Chamon, R. M. Anjos, R. Veiga, M. Dasgupta, D. J. Hinde, and K. Hagino, Phys. Rev. C. **73**, 064606 (2006).

[8] L. F. Canto, P. R. S. Gomes, J. Lubian, L. C. Chaon, and E. Crema, Nucl. Phys. A **821**, 51 (2009).

[9] A. Mukherjee, S. Roy, M. K. Pradhan, M. S. Sarkar, P. Basu, B. Dasmahapatra, T. Bhattacharya, S. Bhattacharya, S. K. Basu, A. Chatterjee, V. Tripathi, and S. Kailas, Phys. Lett. B **636**, 91 (2006).

[10] Pushpendra P. Singh, B. P. Singh, M. K. Sharma, Unnati Gupta, Rakesh Kumar, D. Singh, R. P. Singh, S. Muralithar, M. Afzal Ansari, R. Prasad, and R. K. Bhowmik, Phys. Lett. B **671**, 20 (2009).

[11] D. Singh, Sneha B. Linda, Pankaj K. Giri, Amritraj Mahato, Rahul Tripathi, Harish Kumar, M. Afzal Ansari, N. P. M. Sathik, Rahbar Ali, Rakesh Kumar, S. Muralithar, and R. P. Singh, Phys. Lett. B **774**, 7 (2017); D. Singh, R. Ali, M. Afzal Ansari, K. S. Babu, P. P. Singh, M. K. Sharma, B. P. Singh, R. K. Sinha, R. Kumar, S. Muralithar, R. P. Singh, and R. K. Bhowmik, Phys. Rev. C **81**, 027602 (2010).

[12] Abhishek Yadav, Vijay R. Sharma, Pushpendra P. Singh, Devendra P. Singh, R. Kumar, Unnati, M. K. Sharma, B. P. Singh, R. Prasad, and R. K. Bhowmik, Phys. Rev. C **85**, 064617 (2012); A. Yadav, V. R. Sharma, P. P. Singh, R. Kumar, D. P. Singh, Unnati, M. K. Sharma, B. P. Singh, and R. Prasad, *ibid.* **86**, 014603 (2012).

[13] Rahbar Ali, M. Afzal Ansari, D. Singh, Rakesh Kumar, D. P. Singh, M. K. Sharma, Unnati Gupta, B. P. Singh, P. D. Shidling, Dinesh Negi, S. Muralithar, R. P. Singh, and R. K. Bhowmik, Nucl. Phys. A **968**, 403 (2017); R. Ali, D. Singh, M. Afzal Ansari, M. H. Rashid, R. Guin, and S. K. Das, J. Phys. G **37**, 115101 (2010).

[14] H. C. Britt and A. R. Quinton, Phys. Rev. **124**, 877 (1961).

[15] T. Inamura, M. Ishihara, T. Fukuda, T. Shimoda, and Hiruta, Phys. Lett. B **68**, 51 (1977).

[16] T. Udagawa and T. Tamura, Phys. Rev. Lett. **45**, 1311 (1980); T. Udagawa, D. Price, and T. Tamura, Phys. Lett. B **116**, 311 (1982).

[17] J. Wilczynski, K. Siwek-Wilczynska, J. Van-Driel, S. Gonggrijp, D. C. J. M. Hageman, R. V. F. Janssens, J. Lukasiak, R.H. Siemssen, and S. Y. Van Der Werf, Nucl. Phys. A **373**, 109 (1982).

[18] J. P. Bondorf, J. N. De, G. Fai, A. O. T. Karvinen, and J. Randrup, Nucl. Phys. A **333**, 285 (1980).

[19] M. Blann, Phys. Lett. **27**, 337 (1971).

[20] M. I. Sobel, P. J. Siemens, J. P. Bondorf, and H. A. Bethe, Nucl. Phys. A **251**, 502 (1975).

[21] Harish Kumar, Shuail A. Tali, M. Afzal Ansari, D. Singh, Rahbar Ali, Kamal Kumar, N. P. M. Sathik, Siddharth Parashari, Asif Ali, R. Dubey, Indu Bala, Rakesh Kumar, R. P. Singh, and S. Muralithar, Nucl. Phys. A **960**, 53 (2017).

[22] D. Singh, R. Ali, M. Afzal Ansari, B. S. Tomar, M. H. Rashid, R. Guin, and S. K. Das, Phys. Rev. C **83**, 054604 (2011); D. Singh, R. Ali, M. Afzal Ansari, M. H. Rashid, R. Guin, and S. K. Das, *ibid.* **79**, 054601 (2009).

[23] Kamal Kumar, Tauseef Ahmad, Sabir Ali, I. A. Rizvi, A. Agarwal, R. Kumar, and A. K. Chaubey, Phys. Rev. C **88**, 064613 (2013); **89**, 054614 (2014).

[24] A. Diaz-Torres and I. J. Thompson, Phys. Rev. C **65**, 024606 (2002).

[25] A. Diaz-Torres, I. J. Thompson, and C. Beck, Phys. Rev. C **68**, 044607 (2003).

[26] A. Diaz-Torres, D. J. Hinde, J. A. Tostevin, M. Dasgupta, and L. R. Gasques, Phys. Rev. Lett. **98**, 152701 (2007).

[27] Alexis Diaz-Torres, J. Phys. G **37**, 075109 (2010).

[28] Alexis Diaz-Torres, Comput. Phys. Commun. **182**, 1100 (2011).

[29] Alexis Diaz-Torres and Daanish Quraishi, Phys. Rev. C **97**, 024611 (2018).

[30] Maddalena Boselli and Alexis Diaz-Torres, Phys. Rev. C **92**, 044610 (2015).

[31] G. D. Kolinger, L. F. Canto, R. Donangelo, and S. R. Souza, Phys. Rev. C **98**, 044604 (2018).

[32] D. J. Hinde, M. Dasgupta, B. R. Fulton, C. R. Morton, R. J. Wooliscroft, A. C. Berriman, and K. Hagino, Phys. Rev. Lett. **89**, 272701 (2002).

[33] R. Rafiei, R. du Rietz, D. H. Luong, D. J. Hinde, M. Dasgupta, M. Evers, and A. Diaz-Torres, Phys. Rev. C **81**, 024601 (2010).

[34] H. Morgenstern, W. Bohne, W. Galster, K. Grabisch, and A. Kyanowski, Phys. Rev. Lett. **52**, 1104 (1984).

[35] Pushpendra P. Singh, Abhishek Yadav, Vijay R. Sharma, Devendra P. Singh, Unnati Gupta, Manoj K. Sharma, R. Kumar, K. S. Golda, R. P. Singh, S. Muralithar, B. P. Singh, R. K. Bhowmik, and R. Prasad, J. Phys. Conf. Ser. **282**, 012019 (2011); P. P. Singh, B. P. Singh, M. K. Sharma, Unnati, D. P. Singh, R. Prasad, R. Kumar, and K. S. Golda, Phys. Rev. C **77**, 014607 (2008).

[36] K. Surendra Babu, R. Tripathi, K. Sudarshan, S. Sodaye, B. D. Shrivastava, A. Goswami, and B. S. Tomar, J. Phys. G **29**, 1011 (2003); K. Surendra Babu, R. Tripathi, K.Sudarshan, S. Sodaye, A. Goswami, B. D. Shrivastava, and B. S. Tomar, Nucl. Phys. A **739**, 229 (2004).

[37] Vijay R. Sharma, Abhishek Yadav, Pushpendra P. Singh, Devendra P. Singh, Sunita Gupta, M. K. Sharma, Indu Bala, R. Kumar, S. Murlithar, B. P. Singh, and R. Prasad, Phys. Rev. C **89**, 024608 (2014).

[38] Abhishek Yadav, Pushpendra P. Singh, Mohd. Shuaib, Vijay R. Sharma, Indu Bala, Unnati, Sunita Gupta, D. P. Singh, M. K. Sharma, R. Kumar, S. Muralithar, R. P. Singh, B. P. Singh, and R. Prasad, Phys. Rev. C **96**, 044614 (2017).

[39] Mohd. Shuaib, Vijay R. Sharma, Abhishek Yadav, P. P. Singh, M. K. Sharma, D. P. Singh, R. Kumar, R. P. Singh, S. Murlithar, B. P. Singh, and R. Prasad, Phys. Rev. C **94**, 014613 (2016).

[40] Shuail A. Tali, Harish Kumar, M. Afzal Ansari, Asif Ali, D. Singh, Rahbar Ali, P. K. Giri, S. B. Linda, S. Parashari, R. Kumar, R. P. Singh, and S. Muralithar, Nucl. Phys. A **970**, 208 (2018).
[41] Harish Kumar, Shuail A. Tali, M. Afzal Ansari, D. Singh, Rahbar Ali, Kamal Kumar, N. P. M. Sathik, Asif Ali, Siddharth Parashari, R. Dubey, Indu Bala, Rakesh Kumar, R. P. Singh, and S. Muralithar, Euro. Phys. Jour. A **54**, 47 (2018).
[42] C. Gerschel, Nucl. Phys. A **387**, 297 (1982).
[43] P. K. Rath, S. Santra, N. L. Singh, B. K. Nayak, K. Mahata, R. Palit, K. Ramchandran, S. K. Pandit, A. Parihari, A. Pal, S. Appannababu, Sushil K. Sharma, D. Patel, and S. Kailas, Phys. Rev. C **88**, 044617 (2013).
[44] Sabir Ali, Tauseef Ahmad, Kamal Kumar, Muntazir Gull, I. A. Rizvi, A. Agarwal, S. S. Ghugre, A. K. Sinha, and A. K. Chaubey, Phys. Rev. C **98**, 034603 (2018).
[45] Muntazir Gull, Kamal Kumar, Sabir Ali, Tauseef Ahmad, S. Dutt, I. A. Rizvi, A. Agarwal, and R. Kumar, Eur. Phys. Jour. A **54**, 56 (2018).
[46] J. F. Ziegler, SRIM08, http://www.srim.org/, 2008.
[47] P. M. Strudler, I. L. Preiss, and R. Wolfgang, Phys. Rev. **154**, 1126 (1967).
[48] B. P. A. Kumar, E. T. Subramaniam, K. Singh, and R. K. Bhowmik, FREEDOM - High Speed DAS, SANAI, Trombay, India, 1997.
[49] M. Afzal Ansari, R. K. Y. Singh, M. L. Sehgal, V. K. Mittal, D. K. Avasthi, and I. M. Govil, Ann. Nucl. Energy **11**, 173 (1984).
[50] S. Y. F. Chu, L. P. Ekstrom, and R. B. Firestone, The Lund/LBNL Nuclear Data Search, version 2.0, LBNL, Berkeley, CA,1999, http://nucleardata.nuclear.lu.se/toi/index.asp.
[51] National Nuclear Data Centre, Brookhaven National Laboratory, https://www.nndc.bnl.gov/chart/chartNuc.jsp.
[52] J. F. Ziegler, J. P. Biersack, and U. Littmark, *The Stopping and Range of Ions in Solids* (Pergamon, New York, 1985).
[53] J. F. Ziegler, J. P. Biersack, and M. D. Ziegler, SRIM: The Stopping and Range of Ions in Matter, Chester, Maryland (2008).
[54] N. Bohr, Philos, Mag. **25**, 10 (1913).
[55] H. A. Bethe, Ann. Phys. (Leipzig) **397**, 325 (1930); Z. Phys. **76**, 293 (1932).
[56] F. Bloch, Ann. Phys. (Leipzig) **408**, 285 (1933); Z. Phys. **81**, 363 (1933).
[57] J. Lindhard, M. Scharff, and H. E. Schoitt, Mat. Fys. Medd. Dan. Vid. Selsk. **33**, 1 (1963).
[58] Sunita Gupta, B. P. Singh, M. M. Musthafa, H. D. Bhardwaj, and R. Prasad, Phys. Rev. C **61**, 064613 (2000).
[59] S. Mukherjee, A. Sharma, S. Sodaye, A. Gowswami, and B. S. Tomar, Int. J. Mod. Phys. E **15**, 237 (2006).
[60] P. Moller, J. R. Nix, W. D. Myers, and W. J. Swiatecki, Atom. Data and Nucl. Data Tables **59**, 185 (1995).
[61] S. Raman, C. W. Nestor, and P. Tikkanen, Atom. Data and Nucl. Data Tables **78**, 1 (2001).
[62] D. Singh, Sneha B. Linda, P. K. Giri, A. Mahato, R. Tripathi, H. Kumar, S. A. Tali, S. Parashari, A. Ali, R. Dubey, M. Afzal Ansari, R. Kumar, S. Muralithar, and R. P. Singh, Phys. Rev. C **97**, 064610 (2018).
[63] S. B. Linda, Ph. D. thesis, Central University of Jharkhand, Ranchi, India, 2018.
[64] B. Bindu Kumar, Anil Sharma, S. Mukherjee, S. Chakrabarty, P. K. Pujari, B. S. Tomar, A. Gowswami, S. B. manohar, and S. K. Dutta, Phys. Rev. C **59**, 2923 (1999).
[65] Kamal Kumar, Tauseef Ahmad, Sabir Ali, I. A. Rizvi, A. Agarwal, R. Kumar, K. S. Golda, and A. K. Chaubey, Phys. Rev. C **87**, 044608 (2013).
[66] Manoj Kumar Sharma, Unnati, B. P. Singh, R. Kumar, K. S. Golda, H. D. Bhardwaj, and R. Prasad, Nucl. Phys. A **776**, 83 (2006).
[67] K. Hagino, N. Rowley, and A. T. Kruppa, Comput. Phys. Commun. **123**, 143 (1999).
[68] R. O. Akyuz and A. Winther, in *Proceedings of the International School of Physics "Enrico Fermi", 1979, Nuclear Structure and Heavy-Ion Reactions*, edited by R. A. Broglia, C. H. Dasso, and R. Ricci (North-Holland, Amsterdam, 1981), p. 491.